CrystEngComm

Accepted Manuscript

ROYAL SOCIETY OF CHEMISTRY

www.rsc.org/crystengcomm

CrystEngComm

ARTICLE

$BaGa_4O_7$, a New $A_3BC_{10}O_{20}$ Crystalline Phase: Synthesis, Structural Determination and Luminescence Properties

Received 00th January 20xx,
Accepted 00th January 20xx

DOI: 10.1039/x0xx00000x

www.rsc.org/

Marina Boyer[a], Emmanuel Véron[a], Ana Isabel Becerro,[b] Florence Porcher,[c] Matthew R. Suchomel,[d] Guy Matzen[a] and Mathieu Allix*,[a]

The synthesis, structural determination and luminescence properties of a new barium gallate, $BaGa_4O_7$, are reported. This crystalline material can uniquely be obtained by direct cooling from the molten state. The crystallographic structure was determined using a combination of electron, synchrotron and neutron powder diffraction data. $BaGa_4O_7$ crystallizes in the monoclinic *I2/m* space group with a = 15.0688(1) Å, b = 11.7091(1) Å, c = 5.1429(2) Å and β = 91.0452(2)° and can be described as an original member of the $A_3BC_{10}O_{20}$ family. Atypical for this $A_3BC_{10}O_{20}$ structural framework, $BaGa_4O_7$ is found to contain exclusively divalent and trivalent cations. In order to maintain overall electroneutrality, a disordered defect type partial substitution of gallium and oxygen ions on barium sites occurs within the pentagonal channels of $BaGa_4O_7$. Thanks to the flexibility of this structural framework, $BaGa_4O_7$ can be heavily doped by europium and thus is shown to exhibit a strong orange-red luminescence emission at 618 nm under a 393 nm excitation.

Introduction

Direct crystallization from the melt or from glass is an original alternative to conventional solid state synthesis in order to produce new polycrystalline phases.[1–9] Such an approach can lead to innovative materials, as recently demonstrated in the case of polycrystalline ceramics elaborated by full crystallization from glass which show high transparency both in the visible and near infra-red ranges.[5,8,10] The high transparency of these non cubic materials of micrometer crystals size was explained by the absence of porosity inherent to the synthesis process (crystallization from a fully dense glass), and a limited optical anisotropy (very weak birefringence). Interestingly, these new transparent polycrystalline ceramics can be heavily doped with rare earth ions and present interesting optical or photonic properties competing with single crystal performances. As an example, the transparent polycrystalline $BaAl_4O_7$[5] can be simply prepared by a single heat treatment of the corresponding glass composition, resulting in ceramics showing transparency from the visible range up to 5 µm. When doped with Eu^{2+}, $BaAl_4O_7$ presents efficient scintillating properties[11] with characteristics equivalent to those obtained for CsI:Tl, currently one of the most used scintillator materials.

However, the melting temperature of this pure barium aluminate composition remains very high (above 2000 °C), preventing the practical preparation of large scale at low cost. Starting from the $BaAl_4O_7$ composition, we have therefore considered the substitution of gallium for aluminum since gallate glass compositions and related polycrystalline ceramics can be prepared at lower temperatures compared to aluminate compositions, as recently demonstrated by our group in the case of $Sr_3Ga_2O_6$ compared to $Sr_3Al_2O_6$.[10]

In the BaO-Ga_2O_3 binary system, multiple crystalline phases may offer new opportunities for transparent ceramics materials. Prior to this work, only four different crystalline phases had been reported in the BaO-Ga_2O_3 binary system: $Ba_4Ga_2O_7$,[12] $Ba_3Ga_2O_6$,[13–15] $BaGa_2O_4$[16–19] and $BaGa_{12}O_{19}$.[20,21] These materials were studied either for their ionic conductivity[15] or luminescence properties.[16] Unfortunately, despite a significantly decreased melting temperature into the range accessed by classic furnace at approximately 1500 °C, $BaGa_4O_7$ glass materials cannot be prepared at a large scale, even with the use of fast quenching, as devitrification systematically occurs. Nevertheless, a new barium gallate crystalline phase corresponding to the $BaGa_4O_7$ nominal composition has been identified.

In this present work we report on the synthesis and structure determination from powder diffraction of a new $BaGa_4O_7$ crystalline phase simply prepared by congruent crystallization upon cooling from the melt. We show that this material can be identified as a member of the large $A_3BC_{10}O_{20}$ family which already comprises several members with *A* = Sr, Ba, Pb; *B* = Sn, Ti, Si, Ge, Ta, Bi and *C* = Al, Ga, Fe.[22–31] These materials have been previously studied for their physicals properties: $Ba_6Ga_{21}TaO_{40}$[30] was demonstrated to exhibit an insulator behavior, $Ba_3SiAl_{10}O_{20}$[31] presents a wide emission band centered at 400 nm when doped with cerium and

[a] CNRS, CEMHTI UPR 3079, Univ. Orléans, F-45071 Orléans, France
[b] Instituto de Ciencia de Materiales de Sevilla (CSIC-US), Avenida Américo Vespucio s/n, Isla de La Cartuja, 41092 Sevilla, Spain
[c] Laboratoire Léon Brillouin CEA-CNRS UMR12, CEA/Saclay, 91191 Gif-sur-Yvette Cedex, France
[d] Advanced Photon Source, Argonne National Laboratory, Argonne, Illinois 60439, United States

† Corresponding Authors: mathieu.allix@cnrs-orleans.fr

Electronic Supplementary Information (ESI) available: [DTA of the resulting $BaGa_4O_7$ crystalline phase]. See DOI: 10.1039/x0xx00000x

excited at 254 nm and Cadée *et al.* reported that $(Sr;Ba)_3GeGa_{10}O_{20}$ shows blue luminescence, $Pb_3GeGa_{10}O_{20}$ and $Ba_3TiAl_{10}O_{20}$ yellow emission and $Ba_3SnAl_{10}O_{20}$ orange luminescence under a 254 nm excitation.[22] The *A*, *B* and *C* sites are usually respectively occupied by divalent, tetravalent and trivalent cations. Only a few exceptions have been reported such as (i) $Ba_2BiGa_{11}O_{20}$ for which the extra positive charge brought by Bi^{3+} on the Ba^{2+} site is compensated by the substitution of the tetravalent cation by Ga^{3+}, (ii) $Ba_3Ga_{10.5}Ta_{0.5}O_{20}$ which proposes the replacement of the tetravalent B cation by a mixed occupancy of a pentavalent (Ta^{5+}) and trivalent (Ga^{3+}) species, and (iii) the original $Ba_3Si_2TeZn_6O_{20}$[32] composition showing a mixed composition of divalent (Zn^{2+}), tetravalent (Si^{4+}) and hexavalent (Te^{6+}) cations on *B* and *C* sites.

The new $BaGa_4O_7$ crystalline phase reported in this work can be described as an original $A_3BC_{10}O_{20}$ structure in which the *B* cation is divalent and the overall electroneutrality is respected via the presence of local disorder, *i.e.* substitution of barium by gallium and oxygen atoms, in the barium pentagonal tunnels. The detailed structure of this new $BaGa_4O_7$ crystalline material is described and discussed regarding the necessary overall electroneutrality.

Finally, it is well known that inorganic luminescent materials have found extensive applications in optoelectronics (displays, LEDs, and lasers).[33] Many of the inorganic luminescent materials are obtained after doping different hosts with luminescent lanthanide ions. Herein, we demonstrate that, given its structural flexibility, the $BaGa_4O_7$ structure can be heavily doped with Eu^{3+}. The luminescent properties of this new phosphor are investigated and discussed according to the determined structure.

Results and discussion

Synthesis: Direct cooling from the molten state of $BaCO_3$ and Ga_2O_3 mixed in a 1:2 stoichiometric ratio leads to crystallization of a phase which XRD pattern cannot be indexed from a preliminary search in the ICDD database using a barium gallate composition constraint. Interestingly, broadening the search without any compositional constraints led to a match of our experimental data with $Ba_3Sb_{0.5}Ga_{10.5}O_{20}$[34] (JCPDF 047-0536) which structure was not reported (figure 1).

In order to test the possibility to synthesize our new barium gallate oxide material via a classic solid state route, an *in situ* XRD analysis ranging from room temperature up to the melt of the mixture of the $BaCO_3$ and Ga_2O_3 precursors has been undertaken (figure 1). No evidence of any change of the precursors pattern was observed up to 700 °C. At this temperature, $BaCO_3$ starts to react with Ga_2O_3 to form $BaGa_2O_4$ with Ga_2O_3 excess. Next, from 800 °C to 1000 °C, $BaGa_2O_4$ undergoes a phase transition (from $P6_3$ to $P6_322$ space group[19]). The $BaGa_2O_4$ and Ga_2O_3 phases then remained unchanged up to the melting point at 1440 °C. Finally, crystallization of this new crystalline phase, namely hereinafter $BaGa_4O_7$, could be observed during cooling from the melt. From these results, it appears that cooling from the melt may be the unique way to synthesize the new $BaGa_4O_7$ material. A subsequent differential thermal analysis was performed to check the thermal stability of the resulting $BaGa_4O_7$ crystalline phase (figure SI1). No phase transition or decomposition could be observed before the melting point at 1440 °C, thus demonstrating the good thermal stability of this material.No structural data were available for the $Ba_3Sb_{0.5}Ga_{10.5}O_{20}$ structure that matches the XRD pattern of the new $BaGa_4O_7$ crystalline phase: therefore subsequent structure determination from powder diffraction has been undertaken.

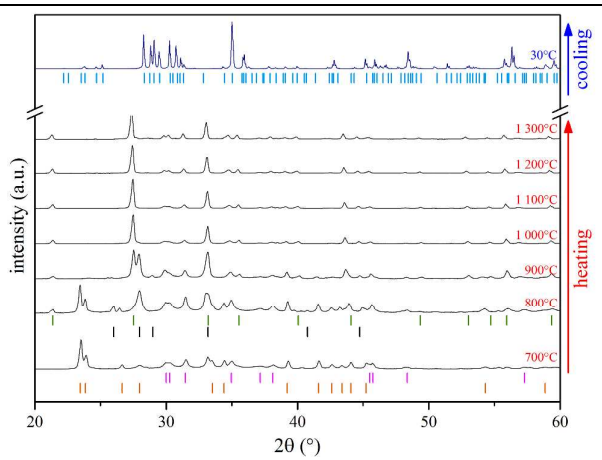

Fig 1: *In situ* X-Ray Diffraction data of the nominal $BaGa_4O_7$ composition from room temperature up to 1300°C. The top dark blue XRD pattern corresponds to the material recorded at room temperature after melting. The different colored marks correspond to the indexation of $Ba_3Sb_{0.5}Ga_{10.5}O_{20}$ (sky blue), $BaCO_3$ (orange), Ga_2O_3 (pink), $BaGa_2O_4$ $P6_3$ (black), and $BaGa_2O_4$ $P6_322$ (in green).

Structure Determination Process: An autoindexing analysis of the synchrotron powder diffraction pattern collected on the new phase of nominal $BaGa_4O_7$ composition was first performed using the DICVOL[35] and TREOR[36] indexing routines. Both softwares led to a unique solution with high figures of merit: M(20)=25 and F(20)=204. The proposed solution is a monoclinic cell with a = 15.05 Å, b= 11.7 Å, c = 5.15 Å and β = 91.07°. A subsequent ICSD database search using similar cell parameters and chemical restrictions (both barium and gallium elements must be present) found only one match, the $Ba_2BiGa_{11}O_{20}$ structure[25] (ICSD 50956 – PDF 89-4705). This monoclinic compound crystallizes in the I2/*m* (n°12) space group and its structure belongs to the $A_3BC_{10}O_{20}$ family, for which several phases (with *A* = Sr, Ba and Pb; *B* = Si, Ge, Sn and Ti and *C* = Al, Ga and Fe) have been previously studied.[22–31]

The structure of $A_3BC_{10}O_{20}$ (figure 2) is based on 12 independent crystallographic sites: 2 sites for *A*, 4 sites shared by *B* and *C* and 6 oxygen sites. Two sites occupied by a mix of *B* and *C* species are forming octahedra (*C*1 and *C*2) and the two others exclusively occupied by *C* type atoms are in a tetrahedral environment (*C*3 and *C*4). Along the *c* axis, $(B/C)O_6$ octahedra form one dimensional pillars via sharing their edges. The CO_4 tetrahedra form a 2D corner sharing tetrahedral sheet perpendicular to the *a* axis. The tetrahedral sheets are linked together by $(B/C)O_6$ octahedral blocks via sharing corners. The linkage of tetrahedral sheets and octahedral blocks form 4, 5 and 6 fold tunnels along the c axis, among which the *A* atom occupies the 5 and 6 fold tunnels such forming chains of cations, and leaving the 4 fold tunnels unoccupied. The pentagonal tunnels are occupied by *A*2 while hexagonal tunnels by *A*1.

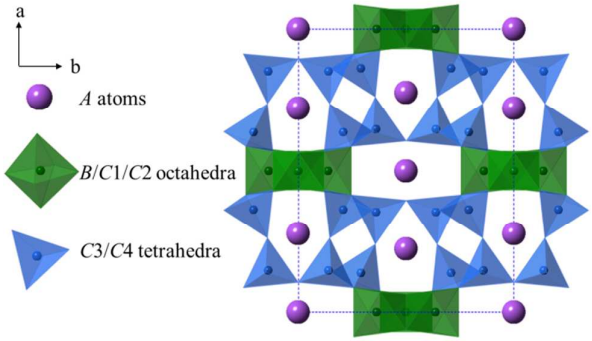

Fig 2: Projection of the $A_3BC_{10}O_{20}$ structure along the c axis. The pink spheres represent A atoms. The $(C3/C4)O_4$ tetrahedra and $(B/C1/C2)O_6$ octahedra are plotted in blue and green, respectively.

The structure of $Ba_2BiGa_{11}O_{20}$ is very similar to the classic $A_3BC_{10}O_{20}$-type compounds, the major difference being that Bi is located in the pentagonal tunnels near the Ba2 site (site occupancy fixed at one-half for each of these two atoms), whereas the *B*-type (*i.e.*, tetravalent) atoms, here one gallium, share sites with *C*1- and *C*2-type atoms. The displacement of the Bi atoms relative to the Ba2 site (around 0.5 Å) was explained by the presence of the stereochemically active $6s^2$ lone pair.

The I2/*m* monoclinic indexation was then tested by performing a LeBail fit of the synchrotron powder diffraction pattern, and the obtained good reliability factors (Rwp = 8.35%, Rp = 6.03%, GOF = 2.80) confirmed the similarity with the $A_3BC_{10}O_{20}$ type structure. The structure elucidation of the $BaGa_4O_7$ phase has then been performed using a combination of synchrotron and neutron powder diffraction data. Rietveld refinement of synchrotron diffraction powder data was first realized using both the cell parameters previously determined and the I2/*m* $Ba_2BiGa_{11}O_{20}$ structure as a starting model. In this preliminary structural model, crystallographic sites of all atoms (two Ba, four Ga and six O sites) were fully occupied and no Bi site was considered, *i.e.* the Ba2 crystallographic site was only considered as fully occupied by Ba, leading to a $Ba_3Ga_{11}O_{20}$ global composition. A reasonable fit could then be obtained, and a subsequent inspection of Fourier difference maps from synchrotron diffraction data revealed two positive residual scattering densities around the Ba2 site on new 4i (*x*, ½, *z*) crystallographic sites (figure 3). These Fourier peaks were assigned to extra gallium sites named Ga5 and Ga6 according to their distances to the nearest-neighbor oxygen atoms within the typical Ga-O bond lengths (1.8 - 2 Å). The presence of two additional gallium atoms close to the Ba2 position (at distances of 1.33 Å and 1.85 Å respectively) would require partial occupancy of this latter as both species cannot be present at the same time. Interestingly, significant negative residual density at the Ba2 position is clearly visible on the Fourier difference map, confirming the Ba2 partial occupancy assumption. The occupancies of Ba2 and of the two extra gallium crystallographic sites were then refined, which resulted in an important improvement of the reliability factors.

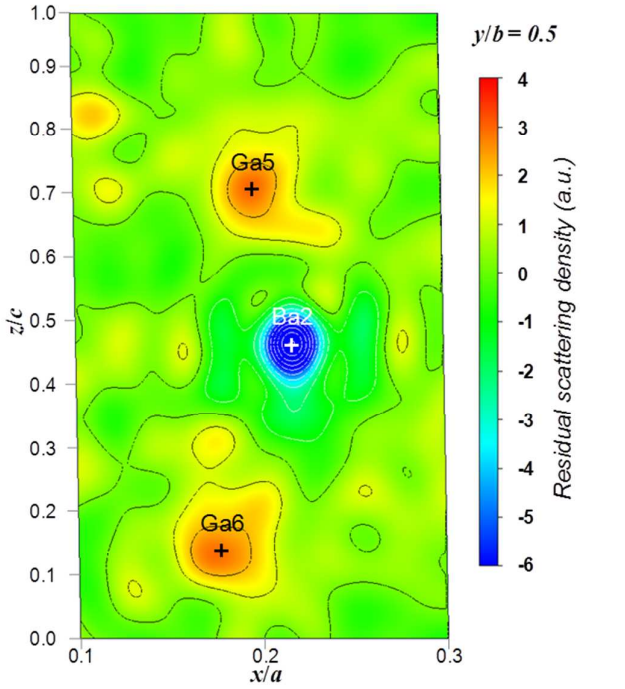

Fig 3: y-axis projection (y/b=0.5) of the Fourier difference map performed after Rietveld refinement of the synchrotron powder diffraction data using the $Ba_2BiGa_{11}O_{20}$ (ICSD 50956)modified structure as a starting model. Residual scattering densities (in arbitrary units) are plotted using 20 levels of contours where solid black and white lines represent positive and negative profiles, respectively. Crosses indicate the further refined atomic positions.

The occupancies obtained for Ba2: 93.1(2)%, Ga5: 8,2(2)% and Ga6: 6,3(2)% are consistent with the presence of two extra gallium atoms coexisting in the pentagonal tunnels instead of a barium atom. It is worth noting that Ga5 and Ga6 have close occupancy values which are complementary to Ba2, which would suppose a full occupancy of the pentagonal tunnels, either by barium (Ba2) or gallium (Ga5 and Ga6).

In order to complete the coordination polyhedra of Ga5 linked to one O1 and two O3 oxygen atoms (with distances of 2.12(1) Å and 1.96(1) Å respectively) and Ga6 linked to two O3 and two O6 oxygen atoms (with distances of 2.21(1) Å and 2.14(1) Å respectively), and given the low Ga5 and Ga6 occupancies a Rietveld refinement based on neutron powder diffraction data was carried out. An oxygen position could be clearly detected using Fourier difference maps. This oxygen atom, labeled O7, is 5.2(12) % occupied and localized on a 4i crystallographic site to a distance of 2.17(12) Å and 1.69(12) Å from additional Ga5 and Ga6 atoms respectively and very closed to the Ba2 atom (0.86(11) Å). In order to prevent instability during the refinement due to the proximity of this new oxygen with the Ba2 atom, the site occupancy of O7, Ga5 and Ga6 were constraint to be equal. With this new insight, the cell parameters, atomic positions, anisotropic thermal parameters, and occupancies for all atoms were refined by the Rietveld method on synchrotron powder diffraction data, leading to the actual

$Ba_{5.73(5)}Ga_{22.53(10)}O_{39.84(15)}$ (*i.e.* $BaGa_{3.93(2)}O_{6.95(3)}$) formula. This formula is consistent with the $BaGa_4O_7$ nominal composition.

The results of the Rietveld refinement show a partial occupation of the O1 crystallographic site (88.5(6)%). This O1 oxygen is bonded to both Ga1 and Ga2 crystallographic positions which are located in an octahedral environment. The presence of vacancies on the O1 site, which was fully occupied in the initial model, is necessary to preserve the electroneutrality of the crystalline structure. However, a local rearrangement of the $Ga1O_4$ and $Ga2O_4$ polyhedra has to be considered, even though this local and limited disorder defects cannot be probed using the average long-range periodic structural information obtained from refinement of these powder diffraction data.

Structural Description: A final refinement was then conducted on the synchrotron powder diffraction data using a same occupation constraint for the Ga5, Ga6 and O7 sites and considering a full occupancy of the pentagonal tunnels, *i.e.* no vacancies (occBa2 + occGa5 = 1). This final refinement was stable and led to good reliability factors (Rwp = 7.66%, Rp= 6.11%, GOF = 1.48) similar to those obtained without constraints. The resulting model was then chosen to describe the structure of the $BaGa_4O_7$ material further in this paper. The Rietveld plot corresponding to the final synchrotron powder diffraction data refinement is shown in figure 4. Table 1 lists the final refined structural parameters for $BaGa_4O_7$. The bond lengths and bond valence sum[37] values calculated for each cation species are given in table 2. The structure of $BaGa_4O_7$, displayed in figure 5, demonstrates the three-dimensional mixed GaO_4 tetrahedral and GaO_6 octahedral framework.

Crystalline structures with similar $A_3BC_{10}O_{20}$ general formula are usually stabilized by an heteroatom (*B*), generally a tetravalent or pentavalent element such as Sn, Ti, Ge, Si, Ta or Bi. Interestingly, the new pure barium aluminate $BaGa_4O_7$ ($Ba_{5.73(1)}Ga_{22.53(2)}O_{39.84(3)}$) material belonging to the $A_3BC_{10}O_{20}$ family is stabilized by the existence of three new 4i sites inside the pentagonal tunnels. More precisely, the structure determination performed from powder diffraction shows the presence of two extra gallium sites (Ga5 and Ga6) distinct of Ba2, with a 8% occupancy, in the pentagonal tunnels usually exclusively occupied by barium or by a mixture of barium and an heteroatom sharing the same crystallographic site. These extra gallium sites form $Ga5O_4$ and $Ga6O_5$ polyhedra connected through an extra O7 oxygen site (figure 5). The 5-coordination of gallium as observed for the Ga6 site is rather unusual, although it has already been observed in the magnetoplumbite-type $BaGa_{12}O_{19}$[20] (mixed GaO_6 and GaO_5 environments) and the recently identified interstitial oxygen conducting melilite $La_{1+x}A_{1-x}Ga_3O_{7+0.5x}$ (*A*=Sr, Ca) (mixed GaO_4 and GaO_5)[38,39]. The results of bond valence sum calculation (listed in table 2) are very closed to the expected ideal values (*i.e.* the respective oxidation numbers), except for Ga5 and Ga6 (1.9(1) and 2.3(2) respectively). As shown in table 2, the mean gallium-oxygen bond lengths of 2.01(2) and 2.09(3) found respectively for $Ga5O_4$ and $Ga6O_5$ polyhedra are within typical range of gallium in octahedral sites (~2 Å), and would indicate that these additional atoms may be slightly underbonded in the proposed model. The

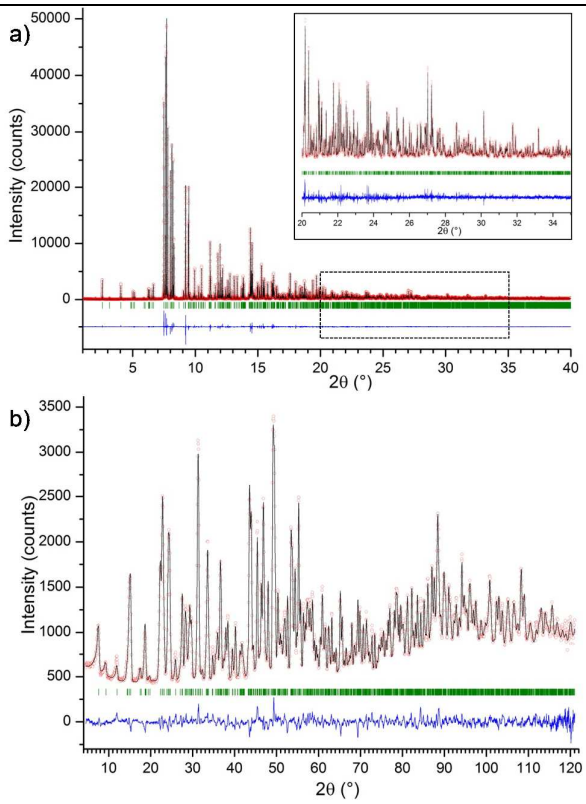

Fig 4: Final Rietveld refinement of (a) synchrotron (R_{wp} = 7.66%, R_p= 6.11%, χ^2 = 1.48) and (b) neutron (R_{wp} = 3.85%, R_p= 3.11%, χ^2 = 2.57) powder diffraction data of $BaGa_4O_7$ collected at room temperature. Observed (red circles), calculated (black line), and difference (blue line) profiles are shown. The set of green vertical lines corresponds to reflection positions. The inset enlarges the synchrotron refinement over the 20-35angular range (2θ).

deviation from the model could be explained by the presence of local rearrangements of the defects in order to accommodate the structure. This local reorganization is most probably taking place locally but is not widely organized across the material as no extra reflections corresponding to a superstructure due to periodic arrangement of barium and extra gallium atoms along the pentagonal tunnels could be observed on the $BaGa_4O_7$ [001]* electronic diffraction pattern (presented figure 6). However, the limited amount of Ga5 and Ga6 compared to the overall gallium content present in the structure prevents further inspection at the local state as ^{71}Ga NMR would enable.[40]

Table 1 : **Final refined structural parameters obtained from synchrotron powder diffraction data collected at room temperature on $BaGa_4O_7$[a].**

atom	site	*x*	*y*	*z*	occupancy	U(eq)
Ba1	2a	0	0	0	1	0.01292(19)
Ba2	4i	0.28241(3)	0	0.02624(8)	0.92*	0.01132(14)
Ga1	2b	0	0.5	0	1	0.0093(3)
Ga2	4h	0	0.63647(5)	0.5	1	0.0112(2)
Ga3	8j	0.35404(3)	0.36166(3)	0.01194(9)	1	0.00766(13)
Ga4	8j	0.13619(3)	0.28670(3)	0.97626(9)	1	0.00908(4)
Ga5	4i	0.2006(5)	0.5	0.7113(16)	0.08*	0.017(2)
Ga6	4i	0.1821(6)	0.5	0.1594(18)	0.08*	0.031(2)
O1	4i	0.4397(3)	0	0.8228(7)	0.83(2)	0.0108(11)
O2	4i	0.9006(2)	0	0.4161(7)	1	0.0153(9)
O3	8j	0.23833(16)	0.3629(2)	0.9111(5)	1	0.0184(7)
O4	8j	0.41687(14)	0.24572(17)	0.8447(4)	1	0.0068(5)
O5	8j	0.85837(15)	0.14498(18)	0.8644(4)	1	0.0094(5)
O6	8j	0.92676(15)	0.3815(2)	0.8069(5)	1	0.0140(7)
O7	4i	0.234(3)	0	0.115(9)	0.08*	0.01[δ]

[a]Space group I2/m, Z = 2, a = 15.06881(2) Å, b = 11.70914(1) Å, c = 5.142855(6) Å, β = 91.04519(6)°, and V = 907.2685 (21) $Å^3$; Rwp = 7.66%, Rp= 6.11%, GOF = 1.48. The occupancy factors for Ba2, Ga6, Ga5 and O7 sites were constrained to conserve charge balance sum (see text).*(occ.Ba2+occ.Ga5=1 and occ.Ga5=occ.Ga6=occ.O7).[δ] Isotropic thermal parameter fixed for O7 oxygen.

Table 2 : **Interatomic Distances and Bond Valence Sum (BVS) calculation in $BaGa_4O_7$.**

Bond length (Å)			BVS	Bond length (Å)			BVS
Ba1 – O2	2.634(3)	x2	1.91(2)	Ga3 – O2	1.836(2)		3.10(2)
Ba1 – O5	2.805(2)	x4		Ga3 – O3	1.810(2)		
Ba2 – O1	**2.608(4)**			Ga3 – O4	1.873(2)		
Ba2 – O3	**2.776(2)**	**x2**	**1.97(1)**	Ga3 – O5	1.814(2)		
Ba2 – O5	**2.782(2)**	**x2**		Ga4 – O3	1.815(2)		
Ba2 – O6	**2.937(2)**	**x2**		Ga4 – O4	1.860(2)		3.01(1)
				Ga4 – O5	1.852(2)		
Ga1 – O1	1.907(4)	x2	3.12(2)	Ga4 – O6	1.848(2)		
Ga1 – O6	2.022(2)	x4		**Ga5 – O1**	**2.118(9)**		
Ga2 – O1	2.045(2)	x2		**Ga5 – O3**	**1.984(5)**	**x2**	**1.9(1)**
Ga2 – O4	1.951(2)	x2	3.11(1)	**Ga5 – O7**	**1.96(5)**		
Ga2 – O6	1.954(2)	x2		**Ga6 – O3**	**2.228(7)**	**x2**	
				Ga6 – O6	**2.158(8)**	**x2**	**2.3(2)**
				Ga6 – O7	**1.70(4)**		

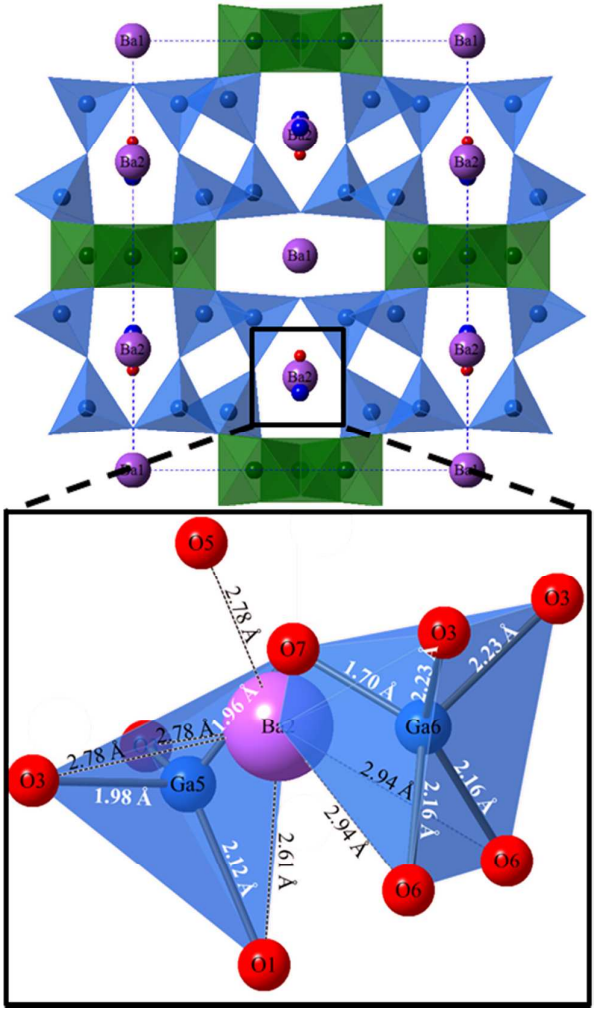

Fig 5: Representation of the defects located in the pentagonal tunnels of the $BaGa_4O_7$ structure. The blue spheres denote the 4-linked Ga5 and 5-linked Ga6 connected together through the new oxygen atoms (O7). The defect corresponds to the presence of the Ga5-O7-Ga6 motif instead of Ba2 (all atoms are present on the scheme for easier understanding).

Luminescence Studies:

In order to analyze the effectiveness of $BaGa_4O_7$ as a matrix to fabricate *Ln*-doped phosphors, $BaGa_4O_7$ was doped with various amounts of Eu^{3+} following the general $Ba_{1-x}Eu_xGa_4O_{7+x/2}$ formulae (x = 0; 0.005; 0.01; 0.05; 0.1; 0.15 and 0.2). Figure 7a presents the XRD patterns recorded on these different compositions. In all the diffractograms, only the $BaGa_4O_7$ crystalline phase is observed. No significant change of the morphology of the crystals could be detected. The line broadening is assigned to chemical disorder due to the substitution of europium within the structure. Moreover, a LeBail refinement performed for each doping level was conducted to determine the cell parameters evolution. This evolution is presented as a function of the doping level in figure 7b. The increase of the europium content clearly leads to a linear decrease of the cell volume, which is in good agreement with a substitution of europium within the $BaGa_4O_7$ crystalline structure as the ionic radius of Eu^{3+} is smaller (0.950 Å and 1.07 Å respectively in the VI

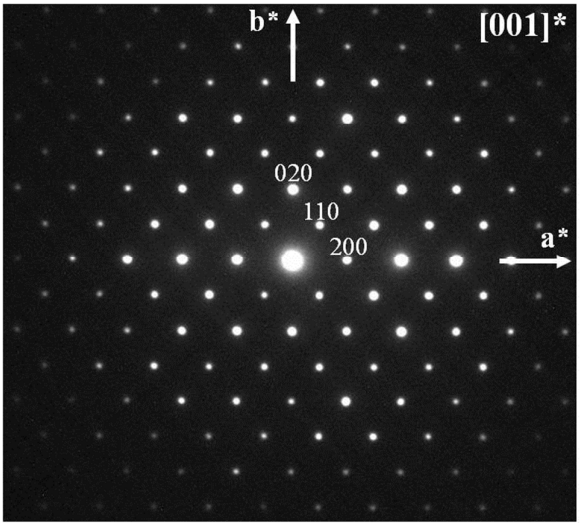

Fig 6: Electron diffraction pattern of $BaGa_4O_7$ oriented along the [001]* direction and showing the I centering of the lattice.

and VIII coordination)[41] than the one of Ba^{2+} (1.36 Å and 1.42 Å respectively in the VI and VIII coordination). It is remarkable to note that $BaGa_4O_7$ can be substituted by large amounts of europium, which can be explained by the flexibility of the structure, especially at the level of the barium pentagonal tunnels as revealed by the Rietveld refinement.

Figure 8 shows the excitation spectrum of the 5% Eu-doped $BaGa_4O_7$ sample taken while monitoring the characteristic Eu^{3+} emission band at 618 nm. The other Eu-doped samples show very similar spectra. The broad band centered at 290 nm is attributed to a charge-transfer transition, which occurs by electron delocalization from the filled 2p shell of the O_2^- to the partially filled 4f shell of Eu^{3+}.[42] The spectrum exhibits as well the typical electronic transitions from the ground state of Eu^{3+} to the *4f* manifold.[43] The latter appear in the 300 - 425 nm range, and have been indexed as labeled on figure 8. The most intense band peaking at 393 nm, corresponding to the $^7F_0 \rightarrow {}^5L_6$ transition, has been used to record the emission spectra of the samples.

The emission spectra of the $BaGa_4O_7$ samples doped with 0.5%, 1%, 5%, 10% and 20% Eu^{3+} recorded after excitation at 393 nm have been plotted in Figure 9. All spectra show the emission lines characteristic of the *4f-4f* transitions of Eu^{3+} ions labeled on the figure. The emission band peaking at 618 nm, due to the electric dipole transition ($^5D_0$-$^7F_2$), appears stronger than the one due to the magnetic dipole transition appearing at 586 nm ($^5D_0$-$^7F_1$). This intensity ratio is characteristic of Eu^{3+} ions located in non-inversion symmetry sites.[44] Although all the emission spectra are very similar to each other in terms of profile and position of the emission bands, it can be observed in Figure 9 that their intensity varies significantly with the Eu content. The inset in figure 9 shows the integrated intensity of the emission spectrum (500 nm - 750 nm) obtained for each composition as a function of the Eu^{3+} doping level. The emission intensity increases linearly with increasing Eu^{3+} content from 0.5% to 5% and reaches a maximum for the $BaGa_4O_7$:5% Eu^{3+}

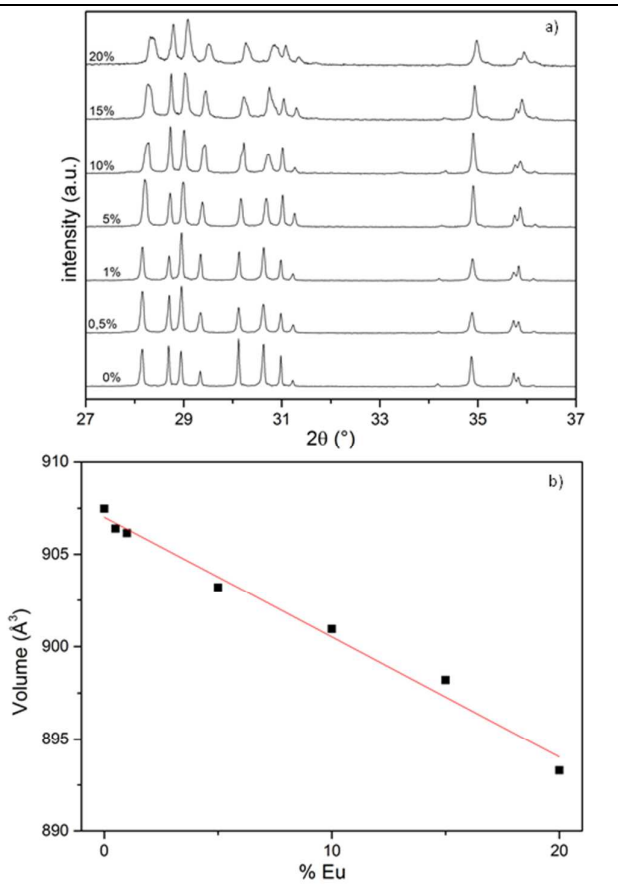

Fig 7: a) Powder XRD data recorded from the doped $Ba_{1-x}Eu_xGa_4O_7$ samples. b) Refined cell volume values obtained from LeBail refinements and plotted as a function of the europium doping ratio.

composition. Further increase of the Eu^{3+} doping level leads to a decrease of the light emission.

The observed augmentation in luminescence intensity is clearly due to the progressive accumulation of emission centers as the doping concentration increases. The decrease in the emission is assigned to a concentration quenching effect, *i.e.* an energy migration between adjacent luminescent centers which becomes significant when the Eu-Eu distance decreases as a result of the increase in doping level.[43,45,46] The optimum Eu doping level corresponds, therefore, to the $BaGa_4O_7$:5% Eu^{3+} sample, in agreement with other matrices described in the literature.[47,48]

The Eu-doped $BaGa_4O_7$ ceramics emit a strong orange-red luminescence under UV radiation with CIE coordinates x=0.59, y= 0.35 for any Eu^{3+} content (Figure 10). This experimental observation together with the high purity of the phase obtained as well as its high thermal stability indicates that Eu-doped $BaGa_4O_7$ could be an interesting material for optoelectronic applications.

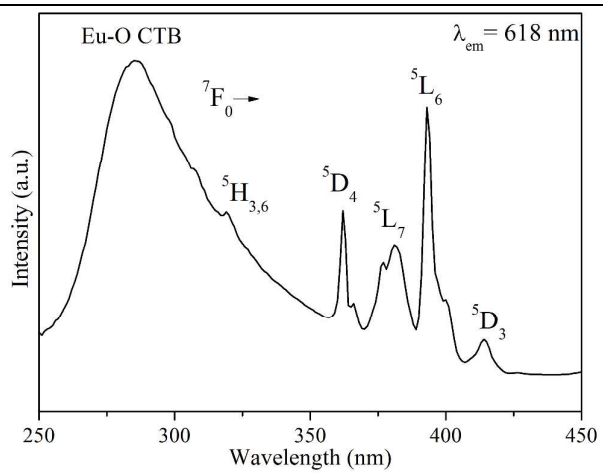

Fig 8: Excitation spectrum of the 5% Eu^{3+}-doped $BaGa_4O_7$ sample at λ_{em}= 618 nm.

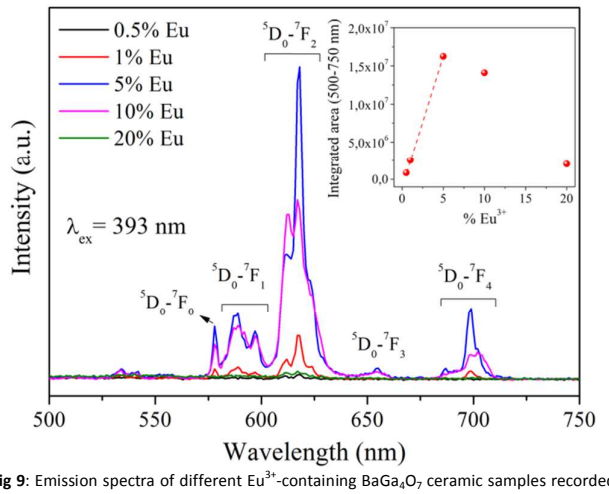

Fig 9: Emission spectra of different Eu^{3+}-containing $BaGa_4O_7$ ceramic samples recorded after excitation at 393 nm. The inset corresponds to the integrated area of the emission spectra of the Eu^{3+}-doped $BaGa_4O_7$ samples as a function of the Eu doping content. The dotted line is given as a guide to the eye.

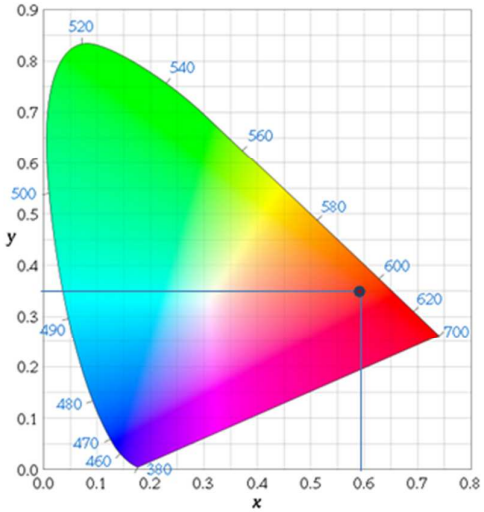

Fig 10: CIE diagram showing the chromatic coordinates (x= 0.59, y= 0.35) of the Eu^{3+}-doped $BaGa_4O_7$ samples analyzed in this work.

Experimental

Synthesis: $BaCO_3$ and Ga_2O_3 high purity powders (99.9% - Strem Chemicals) were first weighed in appropriate amounts using a 1:2 ratio and then mixed together with ethanol in an agate mortar to ensure homogeneity. An excess of $BaCO_3$ (2 wt%) was added to compensate for barium oxide volatilization. Powders were then placed in a platinum crucible in an open air atmosphere furnace and heated up to 1250°C for 12 hours in order to remove carbon dioxide and engage both barium and gallium oxides in mixed oxides to restrain barium volatilization. After subsequent grinding, the powder was heated again at 1475°C for 15 min to ensure melting, and the sample was finally taken out of the hot furnace and cooled down to room temperature. No glass forming could be observed, even when the sample was rapidly quenched in water. The crystalline phase was finally ground to obtain a beige powder. Regarding Eu-doped samples, the Eu_2O_3 (99.99 % - Strem Chemicals) precursor was used to aim for different $Ba_{1-x}Ga_4O_{7+x/2}:Eu_x^{3+}$ compositions following the same protocol.

Differential Thermal Analysis (DTA) was carried out with a Setaram SETSYS Evo 2400 instrument. 50 mg of powder were heated up to 1600°C at 10°C/min under an argon gas flow.

X-ray, Synchrotron, Neutron, and Electron Powder Diffraction: Laboratory X-Ray Diffraction (XRD) was used to control the purity and lattice parameters of Eu-doped $BaGa_4O_7$ samples. Measurements were performed on a D8 Advance Bruker Bragg-Brentano diffractometer (CuKα radiation) equipped with a lynxEye XE detector. Data were collected between 13 and 135° (2θ) at room temperature with a 0.01° step size and a 2 s acquisition time per step.

In situ X-ray diffraction measurements were performed on a D8 Advance Bruker Bragg-Brentano ($CuK\alpha_{1,2}$ radiation) diffractometer equipped with a linear Vantec detector. Powders were placed on a platinum ribbon in a HTK16 Anton Paar chamber. Diffractograms were collected between 15 and 60° (2θ) with a 0.025° step size from room temperature up to the melting point of the sample.

Synchrotron X-ray powder diffraction (SPD) was carried out on beamline 11-BM at the Advanced Photon Source (APS), Argonne National Laboratory. Data collection was acquired at room temperature on powder loaded in a 0.8 mm diameter kapton tube with a wavelength of λ = 0.413705 Å from 1 to 60° (2θ) and a step size of 0.001°.

Neutron powder diffraction (NPD) data were obtained at the Laboratoire Léon Brillouin on the 3T2 diffractometer at room temperature with a 6 mm diameter vanadium tube. Data were collected with a wavelength of λ = 1.2255 Å over the 4.5 to 121° 2θ range with a 0.05 Å step size, for a total of 24 hours acquisition time.

Structure refinements were performed from powder diffraction using the Jana2006 software.[49]

Transmission Electron Microscopy (TEM) data were collected on a Philips CM20 microscope fitted out with an Oxford EDS analyzer. The sample was first crushed in ethanol, and a drop of the solution with the small crystallites in suspension was deposited onto a carbon coated copper grid.

Luminescence of Eu-doped $BaGa_4O_7$ samples: Excitation and emission spectra of the different Eu-doped $BaGa_4O_7$ ($Ba_{1-x}Ga_4O_{7+x/2}:Eu_x^{3+}$) powders were recorded in a Horiba Jobin-Yvon Fluorolog3 spectrofluorometer operating in the front face mode. The CIE color coordinates of the emitted light were calculated from the emission spectra, considering a 2° observer.

Conclusion

A new barium gallate $BaGa_4O_7$ ceramic has been discovered and its detailed structure and luminescence properties are reported. The synthesis of the pure $BaGa_4O_7$ composition is achieved uniquely by direct cooling from the molten state. This phase is stable upon heating up to its melting point at 1440 °C but cannot be obtained from conventional solid state ceramic synthesis. Rietveld refinements performed on both synchrotron and neutron powder diffraction data led to a detailed characterization of the crystalline structure. $BaGa_4O_7$ crystallizes in the *I2/m* monoclinic cell, with a = 15.0688(1) Å, b = 11.7091(1) Å, c = 5.1429(2) Å and β = 91.0452(2)° and can be identified as a member of the $A_3BC_{10}O_{20}$ family. Remarkably, no tetravalent or pentavalent atomic species are necessary as usually required for this family. The structure is here stabilized via the presence of local defects within the pentagonal tunnels. Approximately 10 % of barium sites are occupied by extra gallium and oxygen ions in a complete random manner within the tunnels to ensure electroneutrality of the framework. Remarkably, this new barium gallate material can be easily doped with europium given its structural flexibility, leading to $Ba_{1-x}Ga_4O_7:Eu_x^{3+}$ polycrystalline ceramics showing strong luminescence in the orange-red region under a 393 nm excitation. The optimum Eu^{3+} content is around 5%, which leads to a maximum of emission centers without quenching effect. The high purity and thermal stability of the new phase described make this material an excellent red phosphor for optoelectronic applications. This discovery spotlights an innovative route for exploring new phase space and accessing new polycrystalline compositions via disordered glass or liquid material paths.

Acknowledgements

The authors thank the French ANR for its financial support to the project CrystOG ANR-12-JS08-0002, the Spanish MEC project MAT2011-23593 and the CRMD laboratory for TEM access. Use of the Advanced Photon Source at Argonne National Laboratory was supported by the U. S. Department of Energy, Office of Science, Office of Basic Energy Sciences, under Contract No. DE-AC02-06CH11357. Neutron experiments were performed at the Laboratoire Léon Brillouin in Saclay (France).

Notes and references

1 T. Shishido, Y. T. Zheng, A. Saito, H. Horiuchi, K. Kudou, S. Okada and T. Fukuda, *J. Alloys Compd.*, 1997, **260**, 88–92.

2 I. V. Ogorodnyk, I. V. Zatovsky and N. S. Slobodyanik, *Russ. J. Inorg. Chem.*, 2007, **52**, 121–125.

3 J. Yu, S. Kohara, K. Itoh, S. Nozawa, S. Miyoshi, Y. Arai, A. Masuno, H. Taniguchi, M. Itoh, M. Takata, T. Fukunaga, S. Koshihara, Y. Kuroiwa and S. Yoda, *Chem. Mater.*, 2009, **21**, 259–263.
4 N. Y. Strutynska, I. V. Zatovsky, M. M. Yatskin, N. S. Slobodyanik and I. V. Ogorodnyk, *Inorg. Mater.*, 2012, **48**, 402–406.
5 M. Allix, S. Alahrache, F. Fayon, M. Suchomel, F. Porcher, T. Cardinal and G. Matzen, *Adv. Mater.*, 2012, **24**, 5570–5575.
6 E. Veron, M. N. Garaga, D. Pelloquin, S. Cadars, M. Suchomel, E. Suard, D. Massiot, V. Montouillout, G. Matzen and M. Allix, *Inorg. Chem.*, 2013, **52**, 4250–4258.
7 G. Rousse, B. Baptiste and G. Lelong, *Inorg. Chem.*, 2014, **53**, 6034–6041.
8 K. Al Saghir, S. Chenu, E. Veron, F. Fayon, M. Suchomel, C. Genevois, F. Porcher, G. Matzen, D. Massiot and M. Allix, *Chem. Mater.*, 2015, **27**, 508–514.
9 T. Nakanishi, K. Watanabe, J. Ueda, K. Fushimi, S. Tanabe and Y. Hasegawa, *J. Am. Ceram. Soc.*, 2015, **98**, 423–429.
10 S. Alahrache, K. Al Saghir, S. Chenu, E. Veron, D. D. S. Meneses, A. I. Becerro, M. Ocana, F. Moretti, G. Patton, C. Dujardin, F. Cusso, J.-P. Guin, M. Nivard, J.-C. Sangleboeuf, G. Matzen and M. Allix, *Chem. Mater.*, 2013, **25**, 4017–4024.
11 G. Patton, F. Moretti, A. Belsky, K. A. Saghir, S. Chenu, G. Matzen, M. Allix and C. Dujardin, *Phys. Chem. Chem. Phys.*, 2014, **16**, 24824–24829.
12 V. Kahlenberg, *Z. Für Anorg. Allg. Chem.*, 2001, **627**, 2386–2390.
13 T. Mitamura, H. Ogino, H. Kobayashi, T. Mori and H. Yamamura, *J. Am. Ceram. Soc.*, 1993, **76**, 2127–2128.
14 V. Kahlenberger, *Cryst. Res. Technol.*, 2001, **36**, 319–326.
15 T. Ishihara, H. Matsuda, M. Azmi bin Bustam and Y. Takita, *Solid State Ion.*, 1996, **86–88, Part 1**, 197–201.
16 S. H. M. Poort, W. P. Blokpoel and G. Blasse, *Chem. Mater.*, 1995, **7**, 1547–1551.
17 H.-J. Deiseroth and H. Müller-Buschbaum, *J. Inorg. Nucl. Chem.*, 1973, **35**, 3177–3182.
18 V. Kahlenberg, R. X. Fischer and J. B. Parise, *J. Solid State Chem.*, 2000, **154**, 612–618.
19 V. Kahlenberg and C. Weidenthaler, *Solid State Sci.*, 2002, **4**, 963–968.
20 T. R. Wagner, *J. Solid State Chem.*, 1998, **136**, 120–124.
21 L. Kovba, L. Lykova, V. Kobzareva, L. Lopato and A. Shevchenko, *Zhurnal Neorganicheskoi Khimii*, 1975, **20**, 1970–1973.
22 M. C. Cadée, D. J. W. Ijdo and G. Blasse, *J. Solid State Chem.*, 1982, **41**, 39–43.
23 H. Vinek, H. Völlenkle and H. Nowotny, *Monatshefte Für Chem. Chem. Mon.*, 1970, **101**, 275–284.
24 G. D. Fallon, B. M. Gatehouse and P. J. Wright, *J. Solid State Chem.*, 1985, **60**, 203–208.
25 T. R. Wagner and T. J. Styranec, *J. Solid State Chem.*, 1998, **138**, 313–320.
26 J. Guha, D. Kolar and B. Volavsek, *J. Solid State Chem.*, 1976, **16**, 49–54.
27 M. Cadee, G. Verschoor and D. Ijdo, *Acta Crystallogr. Sect. C-Cryst. Struct. Commun.*, 1983, **39**, 921–925.
28 A. Teichert and H. Müller-Buschbaum, *J. Alloys Compd.*, 1992, **182**, L19–L21.
29 A. Teichert and H. Müller-Buschbaum, *J. Common Met.*, 1991, **170**, 315–320.
30 J. Cao, X. Yu, X. Kuang and Q. Su, *Inorg. Chem.*, 2012, **51**, 7788–7793.
31 W. Konijnendijk, J. Verlijsdonk, W. Vandespijker and G. Boogerd, *J. Am. Ceram. Soc.*, 1979, **62**, 626–627.
32 H.-L. Jiang and J.-G. Mao, *Z. Für Anorg. Allg. Chem.*, 2006, **632**, 2053–2057.
33 E. L. Cates, S. L. Chinnapongse, J.-H. Kim and J.-H. Kim, *Environ. Sci. Technol.*, 2012, **46**, 12316–12328.
34 A. Kaminskii, B. Mill, E. Belokoneva, A. Butashin, S. Sarkisov, K. Kurbanov and G. Khodzhabagyan, *Inorg. Mater.*, 1986, **22**, 1635–1639.
35 A. Boultif and D. Louer, *J. Appl. Crystallogr.*, 1991, **24**, 987–993.
36 P. Werner, L. Eriksson and M. Westdahl, *J. Appl. Crystallogr.*, 1985, **18**, 367–370.
37 I. Brown and D. Altermatt, *Acta Crystallogr. Sect. B-Struct. Sci.*, 1985, **41**, 244–247.
38 X. Kuang, M. A. Green, H. Niu, P. Zajdel, C. Dickinson, J. B. Claridge, L. Jantsky and M. J. Rosseinsky, *Nat. Mater.*, 2008, **7**, 498–504.
39 M.-R. Li, X. Kuang, S. Y. Chong, Z. Xu, C. I. Thomas, H. Niu, J. B. Claridge and M. J. Rosseinsky, *Angew. Chem.-Int. Ed.*, 2010, **49**, 2362–2366.
40 M. Allix, S. Chenu, E. Veron, T. Poumeyrol, E. A. Kouadri-Boudjelthia, S. Alahrache, F. Porcher, D. Massiot and F. Fayon, *Chem. Mater.*, 2013, **25**, 1600–1606.
41 R. Shannon and C. Prewitt, *Acta Crystallogr. Sect. B-Struct. Crystallogr. Cryst. Chem.*, 1969, **B 25**, 925–&.
42 B. S. Tsai, Y. H. Chang and Y. C. Chen, *J. Alloys Compd.*, 2006, **407**, 289–293.
43 G. Blasse and B. C. Grabmaier, *Luminescent materials*, Springer-Verlag, Berlin; New York, 1994.
44 P. A. Tanner, *Chem. Soc. Rev.*, 2013, **42**, 5090–5101.
45 D. Pi, F. Wang, X. Fan, M. Wang and Y. Zhang, *Spectrochim. Acta. A. Mol. Biomol. Spectrosc.*, 2005, **61**, 2455–2459.
46 Y. Cui, X. P. Fan, Z. L. Hong and M. Q. Wang, *J. Nanosci. Nanotechnol.*, 2006, **6**, 830–836.
47 A. I. Becerro, S. Rodriguez-Liviano, A. J. Fernandez-Carrion and M. Ocana, *Cryst. Growth Des.*, 2013, **13**, 526–535.
48 S. Rodriguez-Liviano, N. O. Nunez, S. Rivera-Fernandez, J. M. de la Fuente and M. Ocana, *Langmuir*, 2013, **29**, 3411–3418.
49 V. Petříček, M. Dušek and L. Palatinus, *Z. Für Krist. - Cryst. Mater.*, 2014, **229**.

Table of Content

A new compound $BaGa_4O_7$ was discovered by cooling from the melt. It belongs to the $A_3BC_{10}O_{20}$ family and exhibits strong orange-red luminescence emission when doped by europium.